STUDY OF A HORIZONTAL SEAT SUSPENSION WITH A MODEL OF THE SEATED HUMAN BODY AND ENERGY RECOVERY BRAKING SUBSYSTEM[1]

Igor Maciejewski, Sebastian Pecolt, Andrzej Blazejewski,
Bartosz Jereczek, Tomasz Krzyzynski

Koszalin University of Technology, Faculty of Mechanical Engineering, Koszalin, Poland

e-mail: igor.maciejewski@tu.koszalin.pl; sebastian.pecolt@tu.koszalin.pl;

andrzej.blazejewski@tu.koszalin.pl; bartosz.jereczek@tu.koszalin.pl; tomasz.krzyzynski@tu.koszalin.pl

This article explains the mechanics, control strategies and main applications of a new concept which achieves a balance between energy saving and driver comfort. A physical and mathematical model of a suspension system with energy recovery is presented. It shows practical implementation of the BLDC braking system with energy recovery in a horizontal seat suspension and a detailed simulation analysis of their features and performance. The research involves a specific solution, with a specific BLDC motor, and experimental tests on a laboratory stand. The results of the simulation study using a simplified biomechanical model and experimental studies with human participation are presented.

Keywords: biomechanical model, seat suspension, energy recuperation

1. Introduction

One of the major challenges facing the world today is the energy crisis, which affects various sectors and regions. To address this issue, researchers are exploring new ways of storing and converting electricity which are more efficient and eco-friendlier. Some of the current research topics include developing better batteries (Zhang *et al.*, 2022), reducing power consumption (Farghali *et al.*, 2023), and implementing energy recovery systems (ERS) (Cipoletta *et al.*, 2021; Alhajri *et al.*, 2021). The ERS is mainly designed for the automotive industry (Gabriel-Buenaventura and Azzopardi, 2015; Bravo *et al.*, 2018; Salman *et al.*, 2018) and aims to convert some of kinetic energy into electrical energy. This allows one to power small devices such as sensors and microcontrollers, support the main power source, or store the recovered energy, which helps to lower operational costs. Such a process is called the energy harvesting.

The energy harvesters are devices that can capture and convert different forms of energy into electricity. They are often associated with renewable energy sources, such as solar, wind, thermal and geothermal energy. These sources are widely used in outdoor environments, but they depend on the availability and intensity of natural phenomena (Muscat *et al.*, 2022; Mescia *et al.*, 2014; Sudevalayam and Kulkarni, 2011). Another type of energy harvesters is based on mechanical vibrations, which are ubiquitous in indoor environments, where many machines and devices operate. These harvesters use transducers that transform kinetic energy of vibrations into electrical energy. Such transducers can be classified into three main categories: piezoelectric, electrostatic and electromagnetic, depending on the physical principle of their conversion process.

---

[1]Paper presented during PCM-CMM 2023, Gliwice, Poland

Piezoelectric vibrational energy harvesters have attracted a lot of interest in the recent years, and they have been applied in various fields, such as automotive, biomechanics, human body motion, architecture and construction engineering. These harvesters exploit the piezoelectric effect which is the generation of an electric potential by a material when it is subjected to a mechanical strain. The piezoelectric material deforms when it is exposed to vibrations, and this creates a charge imbalance that produces voltage (Hu *et al.*, 2013). However, piezoelectric harvesters have a limitation in their frequency range, as they work best at frequencies above 1 kHz, while most environmental vibrations are in the range of 1 Hz-100 Hz (Halm *et al.*, 2016). Therefore, piezoelectric harvesters need to be tuned to match the frequency of the vibration source (Priyn *et al.*, 2017). However, mechanical vibrations generated by technical devices, such as engines, can become a source of energy for these transducers.

Piezoelectric harvesters are devices that convert mechanical vibrations into electrical energy. They have benefits of being self-powered, producing relatively high voltage, having small size, and having a high efficiency of energy conversion. However, piezoelectric materials have some drawbacks, such as variable power output over time, which affects their performance (Fastier- -Wooller *et al.*, 2022), and possible damage due to brittleness of the material (Matak, 2013; Beeby *et al.*, 2006). Electrostatic transducers are devices that generate voltage by changing their internal capacitance under an applied force (Zhu *et al.*, 2010b). Electrostatic technology includes electret-based vibration energy harvesting using MEMS, which are micro-scale mechanical systems, and triboelectric energy harvesting (Toshiyyoshi *et al.*, 2019). Electrostatic transducers usually need a high-voltage power source or an electret, which is a material that has a permanent electric charge or dipole polarization, to create strong electric fields that drive the electric current, which makes these systems more complex (Zhu *et al.*, 2010a). Moreover, since the gap between capacitor plates or surfaces is typically in a millimetre range, they are not suitable for higher amplitude vibrations without an additional system that adapts the input vibration motion to the appropriate amount of amplitude (Beeby *et al.*, 2006).

Electromagnetic vibrational energy harvesters (EVEH) are devices that convert low- -frequency vibrations into electrical power using the principle of electromagnetic induction. They have a simple structure and can operate in various environments, which makes them attractive for many applications (Araujo and Nicoletti, 2015). For example, EVEH can be used to power wireless sensors, wearable devices, biomedical implants, or environmental monitoring systems. The basic mechanism of EVEH is that a magnet moves relative to a coil and induces an electric current according to Faraday's law (Bouendeu *et al.*, 2011). Another way to achieve electromagnetic energy conversion is by using inverse magnetostrictive materials which change their magnetization state when subjected to mechanical stress. By applying a bias magnetic field with permanent magnets, the strain-induced magnetic flux variation can be captured by a coil and converted into electricity (Akinaga, 2020; Ueno, 2019). Moreover, some vibration energy harvesters combine piezoelectric and electromagnetic effects to enhance their performance. Depending on their configuration, they can be classified into mono-stable, bi-stable, multi-stable, magnetic-plucking (contactless), or hybrid piezoelectric-electromagnetic energy harvesters (Jiang *et al.*, 2021).

Vibrations produced by devices in operation can be a source of energy replenishment. Researchers employ additional components to capture this energy, such as the piezoelectric vibrator proposed in work (Wang, 2020) as an energy converter from track vibrations caused by vehicle movement. The author developed a dynamic model of a vehicle coupled vertically to estimate displacements that affect the piezoelectric element in charge of energy recovery. The researcher then performed simulation tests and concluded that larger displacement amplitudes increase the amount of energy recovered. The vehicle speed and position of the piezoelectric elements also influence the maximisation of the energy output.

Another way to enhance the energy efficiency of automobiles was proposed by Hassan Fathabadi in his article (Fathabadi, 2019). He suggested two modifications: embedding electric coils in shock absorbers to capture and convert vibration energy into a steady DC voltage and adding a wind turbine to the vehicle condenser. The author showed that those two modifications could increase the energy production of electric vehicles and extend their travel range.

Alternatively, energy can be harvested by using the Energy Restore Braking System (ERBS) (Li *et al.*, 2021; Liu and Zhang, 2021). This concept involves converting kinetic energy of motors into electrical energy during deceleration (Taut *et al.*, 2013). This technique is commonly applied in electric vehicles. However, it often needs additional components in the system such as DC-DC converters, which are devices that convert the direct current (DC) from one voltage level to another (Kim, 2011; Onar and Khaligh, 2012), super-capacitors, which are high-capacity capacitors that can store and release large amounts of energy quickly and release it when connected to a chosen circuit (Naseri *et al.*, 2017; Song *et al.*, 2014), or gear shifts, which are mechanisms that change the speed ratio between the motor and wheels (Yang *et al.*, 2007). These components add to the weight and complexity of the system.

Another way to make energy recovery systems more simple is to use a single-stage converter that controls the BLDC motor, as suggested by Godfrey and Sankaranarayanan (2008). This method can switch to the regenerative braking mode by sending switching pulses in a specific sequence. This method does not need extra power converters, which is a benefit compared to other solutions. The authors of (Godfrey and Sankaranarayanan, 2008) present different switch topologies, such as H-bridge, half-bridge and full-bridge, and plugging combined to create a new braking strategy. The switch topologies determine how the current flows through motor windings and how the back electromotive force is generated. The simulation and experimental tests were done to show the effectiveness of the proposed solution.

On the contrary, this article explores how to combine the driver seat suspension system with a special BLDC motor braking system that can turn horizontal vibrations of the driver seat suspension into electric power. The stored power can be used for different vehicle subsystems as needed. This solution also helps one to optimize the active seat suspension systems that use electric motors to create vibration damping force. The idea is to use the motor as a generator to produce this force. The proposed suspension system can be tested using human biomechanical models (Maciejewski *et al.*, 2023). The model gives quick results on the power and vibration levels that affect the driver body parts, which allows for evaluating and comparing different suspension systems.

The first part of the article explains the mechanics, control strategies and main applications of this new concept, which achieves a balance between energy saving and passenger comfort. A physical model and a mathematical model of the suspension system with energy recovery are presented. This approach is based on multiple objectives aiming to accomplish. One of them is to enhance comprehension of complex interactions involved in the seat suspension that can reduce horizontal vibrations affecting comfort and health of work machine operators. Another one is to explore the efficiency and feasibility of incorporating energy recovery mechanisms into these systems, considering both the environmental demands of energy efficiency and the psychophysical health of drivers, operators and passengers. The next subsections of the article present practical implementation of the BLDC braking system with energy recovery in horizontal seat suspension and a detailed simulation analysis of their features and performance. Further research involves simulation analysis of a specific solution, with a specific engine (BLDC motor), and experimental tests on a laboratory stand. The data gathered during experiments can be used to broaden the knowledge about this type of systems and their practical applications. It will suggest the direction of further research, including the use of suitable biomechanical models.

2. Physical and mathematical model

Figure 1 shows the physical model of an active seat suspension and simple biomechanical human body model. The upper part of the human body is modelled as a lumped three mass system (roughly corresponds to the pelvis, torso and head) (Maciejewski *et al.*, 2022b). That inertial system responds to the external excitation x_s. In detail, the first mass m_1 represents the seat frame with pelvis, the cushions and motor inertia, the second mass m_2 represents the body part on the seat back rest, i.e the torso and the third mass m_3 represents the body part that moves freely, i.e. the head. Its mass m_3 has no contact with the backrest. The stiffnesses c_{12}, c_{23}, c_2
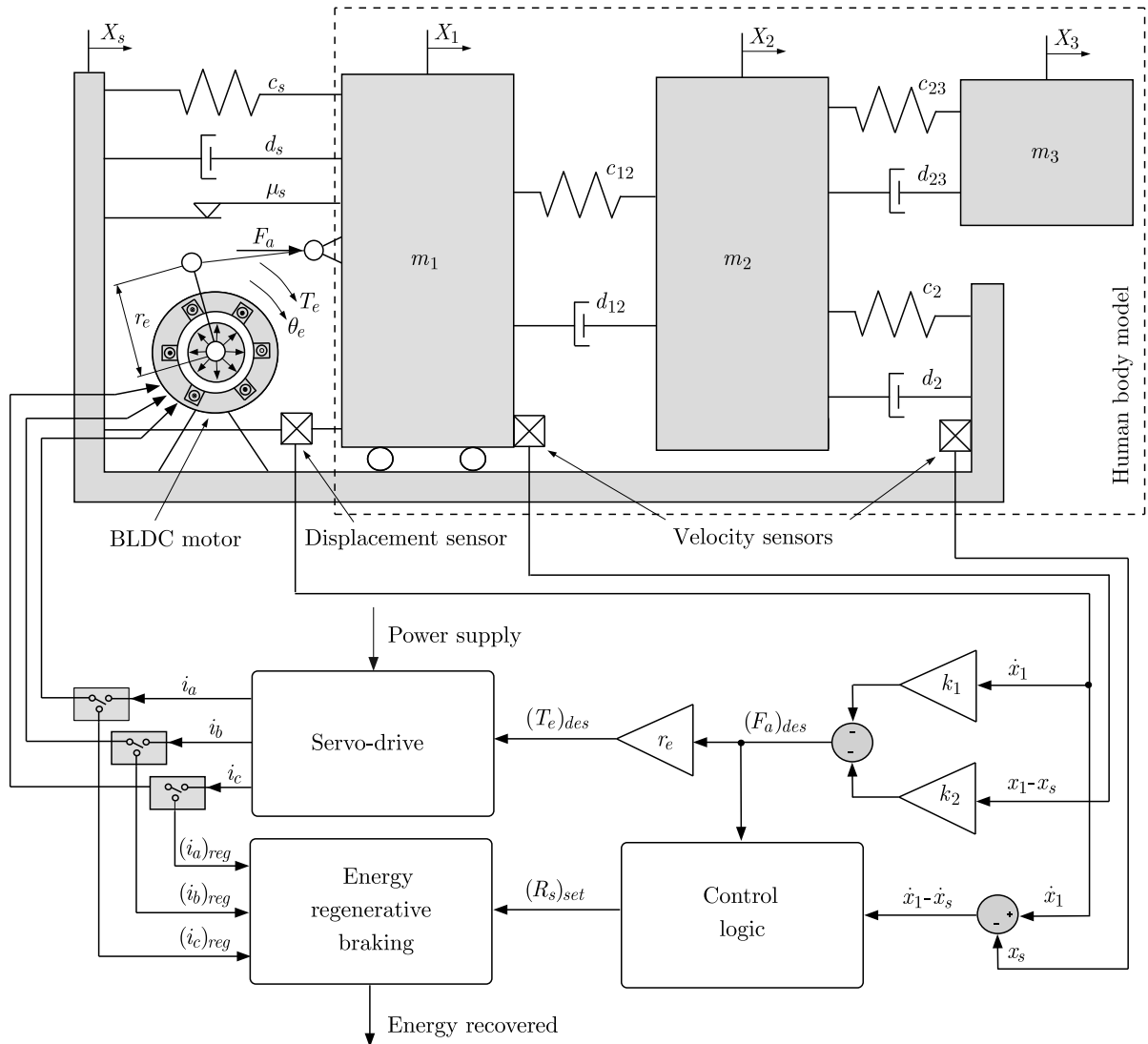

Fig. 1. Physical model of an active seat suspension with the BLDC motor

and damping coefficients d_{12}, d_{23}, d_2 capture visco-elastic properties of the human body tissues. Due to topology and simplicity of the model to identify the above-mentioned parameters, it was necessary to conduct experimental research with human participation and then the carry out the optimisation process. During the experiment, the tested individual was subjected to action of test vibration in the sitting position on the cushioned seat, occupied in the way providing the backrest contact. The identification process was conducted minimising by the error between numerically simulated and experimentally measured transmissibility functions over the frequency range of

1 Hz-12 Hz and introducing the Root Mean Square Error method. A detailed description of the model and its parameter sensitivity analysis is given in the work (Maciejewski *et al.*, 2022b).

This model structure and its proper parameters can be used to predict the biodynamical response of the seated human body in the frequency range of 1 Hz to 12 Hz. The model of the suspension system consists of a human body mass that is attached to two tension springs with stiffness c_s and a damper with damping ratio d_s. The friction in the suspension mechanism is modelled by a coefficient μ_s, which is determined experimentally for a specific seat type and described in the work (Jereczek *et al.*, 2022). Modern seat suspension systems are active systems. The aim of the active subsystem is to minimise harmful vibrations of the body mass. The active element here is a brushless DC motor (BLDC). Such an electric actuator generates an active force F_a which, in turn, is proportional to the electromagnetic torque T_e of this motor. The torque T_e is controlled by a servo-drive mode. The equations of motion for the mechanical structure are given by

$$
\begin{aligned}
m_1\ddot{x}_1 &= -d_s(\dot{x}_1 - \dot{x}_s) - c_s(x_1 - x_s) - \mu_s(m_1 + m_2 + m_3)g\,\mathrm{sgn}\,(\dot{x}_1 - \dot{x}_s) + F_a \\
&\quad + d_s(\dot{x}_1 - \dot{x}_s) + c_s(x_1 - x_s) \\
m_2\ddot{x}_2 &= -d_{12}(\dot{x}_2 - \dot{x}_1) - c_{12}(x_2 - x_1) + d_{23}(\dot{x}_3 - \dot{x}_2) + c_{23}(x_3 - x_2) \\
&\quad + d_2(\dot{x}_s - \dot{x}_2) + c_2(x_s - x_3) \\
m_3\ddot{x}_3 &= -d_{23}(\dot{x}_3 - \dot{x}_2) - c_{23}(x_3 - x_2)
\end{aligned}
\tag{2.1}
$$

Active force F_a in the suspension system is provided by three-phase currents (i_a, i_b and i_c) flowing through stator windings in the presence of a magnetic field from permanent magnets. The resulting force coming from an electric motor is therefore defined as the following function

$$
F_a = \frac{p\lambda}{r_e}(\Phi_a i_a + \Phi_b i_b + \Phi_c i_c)
\tag{2.2}
$$

where: p is the number of pole pairs, λ is the amplitude of flux induced by permanent magnets, r_e is the lever arm of the motor, Φ_a, Φ_b and Φ_c are three-phase electromotive forces. The phase electromotive forces are assumed to be trapezoidal for most of the BLDC motors (Krause *et al.*, 2002).

The trapezoidal model is based on the assumption that the winding distribution and the magnetic flux created by permanent magnets generate three trapezoidal back electromotive forces. The back electromotive forces are the voltages induced in the stator windings by the changing magnetic field. The set of equations that describe the actual motor currents can be written in the phase reference frame (*abc* frame) as follows (Krause *et al.*, 2002)

$$
\begin{aligned}
\dot{i}_a &= \frac{1}{3L_s}[2v_{ab} + v_{bc} - 3R_s i_a + \lambda p\dot{\theta}_r(-2\Phi_a + \Phi_b + \Phi_c)] \\
\dot{i}_b &= \frac{1}{3L_s}[-v_{ab} + v_{bc} - 3R_s i_b + \lambda p\dot{\theta}_r(\Phi_a - 2\Phi_b + \Phi_c)] \\
\dot{i}_c &= -(\dot{i}_a + \dot{i}_b)
\end{aligned}
\tag{2.3}
$$

where: L_s is the inductance of stator windings, v_{ab} and v_{bc} are the phase to phase supply voltages, R_s is the resistance of stator windings. The currents in Eq. (2.3) need to get values that allow reducing the unwanted seat movements. The double-feedback loop system (Maciejewski *et al.*, 2020) is used to calculate the proper, desired active force $(F_a)_{des}$, which is needed to balance the kinematic excitation x_s.

The motor windings currents should produce the desired active force given by the following formula

$$
(F_a)_{des} = \begin{cases} -k_1\dot{x}_1 - k_2(x_1 - x_s) & \text{for} \quad (F_a)_{des}(\dot{x}_1 - \dot{x}_s) \geqslant 0 \quad \leftarrow \text{motoring} \\ 0 & \text{for} \quad (F_a)_{des}(\dot{x}_1 - \dot{x}_s) < 0 \quad \leftarrow \text{braking} \end{cases}
\tag{2.4}
$$

where $\dot{x}_1$ is the absolute velocity of the suspended body given by the mass acceleration sensor (after integration process) (Fig. 1), $x_1 - x_s$ is the relative displacement of the seat suspension measured by the displacement sensor (Fig. 1) k_1 and k_2 are the coefficients feedback that affect significance of reducing velocity of seat vibration (influence of vibration velocity criterion) and significance in limiting the suspension travel (influence of seat displacement criterion), respectively. Formula (2.4) also shows the conditions for which the damping force is generated in the active suspension cycle ("motoring"). and the force is not generated in the energy recovery cycle ("braking").

3. Energy recovery capabilities during braking mode of an induction motor

The force/velocity possibilities of the suspension system are represented as a velocity versus active force graph containing of four quadrants (Fig. 2). This figure illustrates four-quadrant operation of the horizontal seat suspension driven by an induction motor. In the chosen horizontal
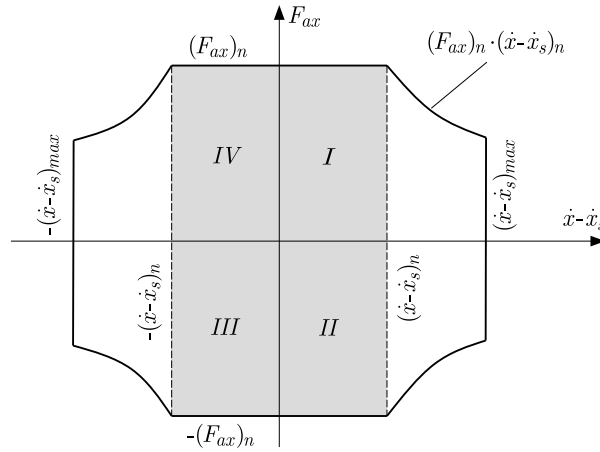
Fig. 2. Four-quadrant operation of the horizontal seat suspension driven by an induction motor

x direction, a constant force $(F_{ax})_n$ is given in grey colour region from 0 to nominal velocity $\pm(\dot{x}_1 - \dot{x}_s)_n$. The rest region (white colour) indicates a significant decrease of the force $(F_{ax})_n$ while an increase of velocity from the nominal $(\dot{x}_1 - \dot{x}_s)_n$ to the maximum value $(\dot{x}_1 - \dot{x}_s)_{max}$. Such a region is limited by a constant power level $(F_{ax})_n(\dot{x}_1 - \dot{x}_s)_n$ due to lowering of the motor magnetic flux. In the first (I) and third quadrant (III), the active force F_{ax} and the velocity $\dot{x}_1 - \dot{x}_s$ have the same signs, indicating the driving mode since the electric force is in the direction of motion. In the second (II) and fourth (IV) quadrant, the active force F_{ax} is opposite to the velocity $\dot{x}_1 - \dot{x}_s$, therefore the braking mode of an induction motor is applied. Operation in these quadrants means that the kinetic energy of the induction motor coupled to a mechanical load can be transformed into the electric energy. The control algorithm that corresponds to possible energy transfer between mechanical and electrical subsystems is defined as follows

$$(R_s)_{set} = \begin{cases} 0 & \text{for} \quad (F_{ax})_{des}(\dot{x} - \dot{x}_s) \geqslant 0 \quad \leftarrow \text{motoring} \\ \max\left[0, \min\left(\left|\dfrac{(F_{ax})_{des}}{\dot{x} - \dot{x}_s}\right|, k_{max}\right)\right]|\dot{x} - \dot{x}_s| & \text{for} \quad (F_{ax})_{des}(\dot{x} - \dot{x}_s) < 0 \quad \leftarrow \text{braking} \end{cases}$$

(3.1)

where: $(R_s)_{set}$ is the controllable external resistance of the induction motor, k_{max} is the constant coefficient representing the maximum braking force of the induction motor, the same BLDC motor working as a generator. Each constant model parameter of the seated human body together

with the horizontal seat suspension and energy recovery braking subsystem is specified in Appendix A.
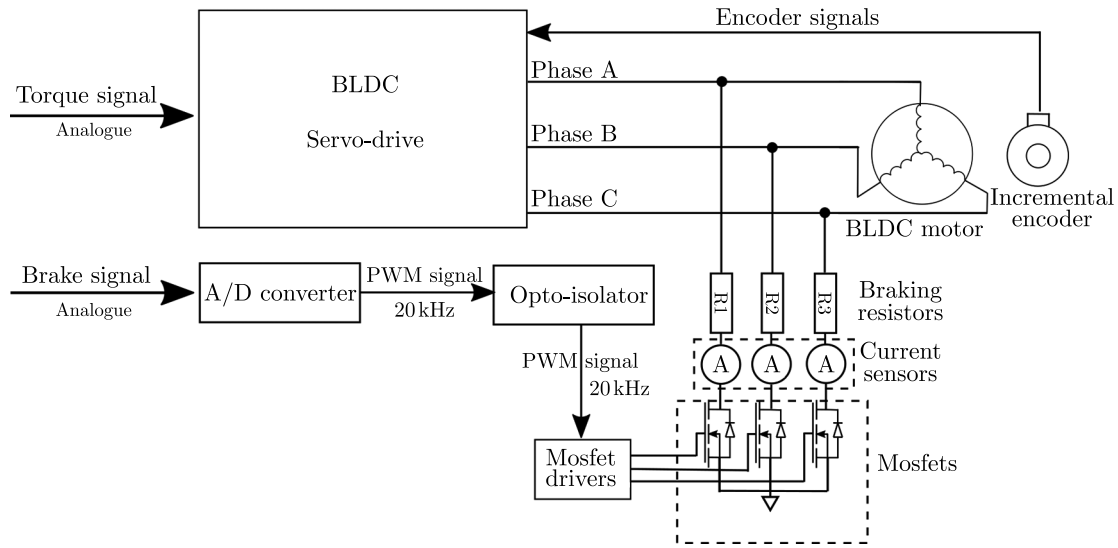

Fig. 3. Regenerative braking system for motor control

Physically, the braking system of the BLDC motor, realising energy transfer, works using resistors and transistors shown in Fig. 3. The system controller sends an analogue "braking" signal to initiate the braking process. This is happening when the controller gets a signal from seat velocity sensor and a torque signal, and calculates according to Eq. (3.1), which means second (II) and fourth (IV) quadrant (Fig. 2). The "braking" signal is converted into a digital PWM form with a frequency of 20 kHz. The PWM signal is then isolated from the transistors using an opto-isolator circuit. The transistors are connected to three braking resistors R_1, R_2 and R_3 which are also connected to the three motor phases A, B and C. When the transistors are turned on by the PWM signal, the motor phases are shorted through the resistors, which creates a braking torque on the BLDC motor. The currents flowing through the motor windings are measured by current sensors based on the Hall effect, which allows us to calculate the power dissipated by the resistors. In the same way, the available energy is determined.

4. Experimental versus simulation results

In the last phase of the research, experimental verification of the correctness of the model, simulation results and the effectiveness of the proposed energy recovery concept in such a system was carried out. The effectiveness and efficiency of the energy harvesting in the horizontal suspension systems was evaluated using the experimental set-up shown in Figs. 4a and 4b. As the physical model assumed, the suspension system (seat suspension system – Fig. 4a) was attached to a base platform (vibrating platform – Fig. 4a), driven by a PMSM motor (vibrations source motor PMSM – Fig. 4b) that produced a random vibration signal with a programmable electro-hydraulic shaker. Finally, the oscillatory seat motion transited to the mass (mass load – Fig. 4a, respectively mass m_1 – Fig. 1) was induced by an active force generated by the PMSM motor through a two-link mechanism. This mechanism transformed the rotational motion of the motor into the translational motion of the suspension system in the longitudinal direction. The accelerometer (platform acceleration sensor – Fig. 4a) was utilised to measure the input signal that was random vibration having a frequency between 0.5 Hz and 12.5 Hz. The data obtained from this accelerometer was recorded by a PC-based data acquisition system with the sampling

time of 1 ms. The output signal was measured by an accelerometer fixed to the mass (mass acceleration sensor – Fig. 4a). The recorded acceleration signals from both accelerometers were simultaneously digitally integrated to obtain velocities of the platform and mass. The rigid mass (mass load – Fig. 4a) was placed on the upper part of the suspension mechanism to load the system to simulate the driver (operator) presence during investigation. The element of the active seat suspension was the brushless motor (BLDC motor – Fig. 4b). Its task was, on the one hand, to generate an active vibration damping force in accordance with the selected algorithm in the control strategy (one of the control algorithms developed by the authors was presented in the work (Maciejewski *et al.*, 2022a), and, on the other hand, to obtain seat vibration energy and convert it into electrical energy, in accordance with the energy acquisition strategy. On the test stand, the energy of the seat movement (longitudinal vibrations) was transferred to the motor through a system of rigid rods and an eccentric system (centrifugal transfer of motion from the seat to the BLDC motor – Fig. 4b). To measure the amplitude of longitudinal seat vibrations directly, a dedicated displacement sensor was used (seat displacement sensor – Fig. 4a). Mounting this sensor enabled measuring the relative displacement of the platform and the seat.
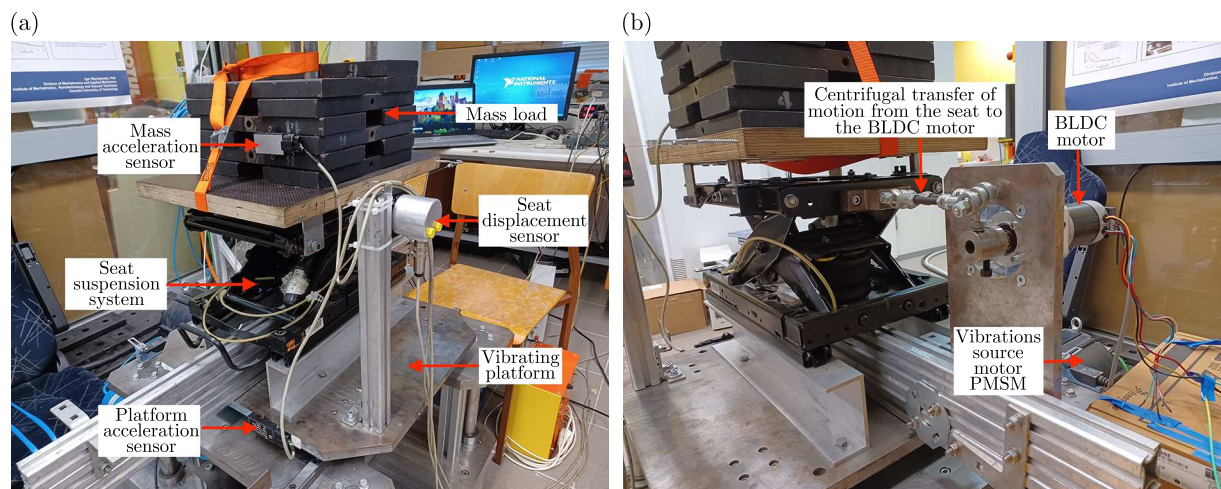

Fig. 4. Actual, overall view of: (a) the test rig with basic sensors, (b) the test stand with a BLDC motor (energy recovery) and a seat vibration motor

The aim of the experimental study was to examine the effect of the tested regenerative system on the suspension performance. Two common factors were selected for the analysis. The first one was the SEAT factor, which measured the seat isolation efficiency. The second one was the suspension travel (relative displacement), which evaluated the seat dynamic response (Maciejewski *et al.*, 2014). Generally, when the SEAT factor was higher than 1, the vibrations were amplified and transmitted from the road to the driver or operator. When the SEAT factor was lower than 1, the vibration isolation improved as the SEAT decreased. For the second factor, a smaller value was preferable. It ensured that the seat did not reach its movement limits when driving on rough roads. The test was carried for a chosen mass value (Mass load 80 kg). Figure 5 shows the tested person of weight 80 kg on the test rig. The same person was tested on passive, active and regenerative seat suspension configuration.

The comparative results of the passive, active and energy regenerative suspension are presented in Table 1. The data in this table show that the use of an energy recovery system generally reduces the vibration-insulating properties of the suspension in caparison to the active one. However, the reduction is approximately 18.1% for this particularly load mass, calculated on the basis of the SEAT factor. However, the dynamic response, calculated on the basis of the suspension travel value, is reduced by approximately 23.6% for the weight of 80 kg. At the
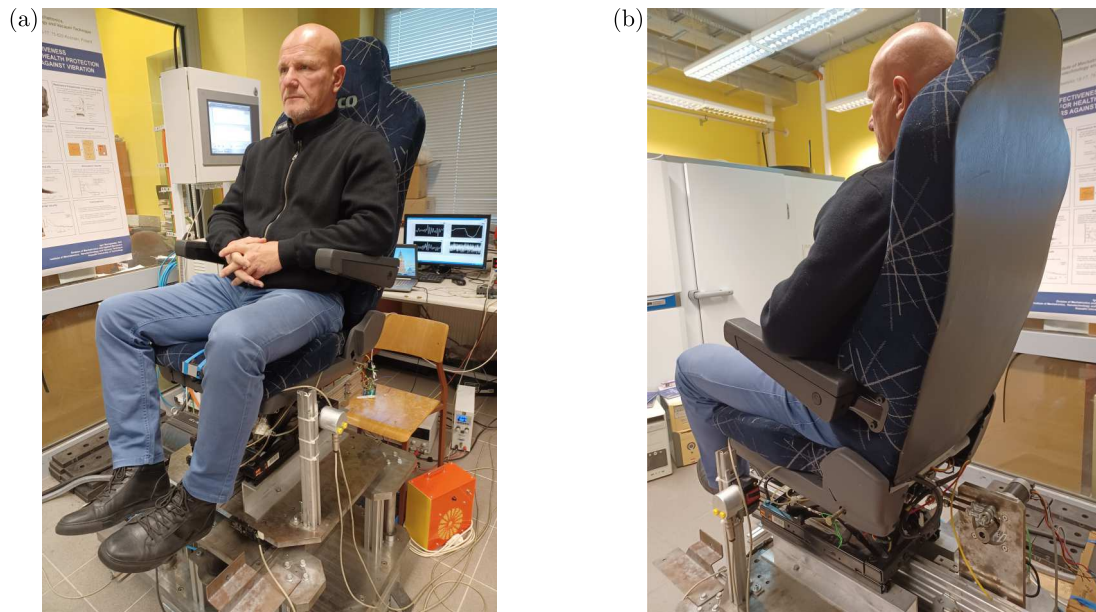
Fig. 5. The view of: (a) the front test rig with the tested person, (b) the rear part with the regenerative system

Table 1. Measured SEAT factors and suspension travels of the passive, active and regenerative suspension system for the mass load of 80 kg

| | Horizontal seat suspension | | | | | |
| | Passive | | Active | | Regenerative | |
Human weight	SEAT factor	Suspension travel	SEAT factor	Suspension travel	SEAT factor	Suspension travel
80 kg	0.877	29.3 mm	0.629	33.5 mm	0.743	25.6 mm

same time, as the values in the first two columns of Table 1 show, such a system still has better vibration isolation properties and dynamic response than the passive one.

At the same time, simulation tests were carried out using a biomechanical human model and a suspension system model. The results of the simulation using the biomechanical model are presented in Table 2. As can be seen from the values presented there, the model gives the same assessment of the vibro-isolation with the SEAT coefficient and the suspension travel value. All values obtained from the model are larger than those from the experiment. The greatest compliance is found in the case of the active suspension system. The largest relative error of the model in the case of SEAT was max 10%. However, in the case of suspension travel, the error reached 15%.

Table 2. Simulated SEAT factors and suspension travels of the passive, active and regenerative suspension system for a mass load of 80 kg

| | Horizontal seat suspension | | | | | |
| | Passive | | Active | | Regenerative | |
Human weight	SEAT factor	Suspension travel	SEAT factor	Suspension travel	SEAT factor	Suspension travel
80 kg	0.923	32.7 mm	0.630	35.5 mm	0.816	29.3 mm

In detail, the range in which an energy recovery suspension system works better than a passive system can be indicated by analysing power spectral densities (Fig. 6a) and transmissibility

functions graphs (Fig. 6b). The curves of both types of functions, for this case of mass load, indicate the frequency limit of 3 Hz. Below this frequency, the active and regenerative system represents similar vibro-isolation properties. The graph shows slightly better properties of the active system. In that frequency limit, the passive system demonstrates clearly inferior properties. In the case of frequencies above 3 Hz, the two systems, passive and regenerative, show similar vibration isolation properties and much worse than for the active one. However, as the transmissibility function curve for the regenerative system shows (Fig. 6b), it is below the value of 1 throughout the frequency range. Therefore, it significantly reduces vibrations coming from the ground or road.
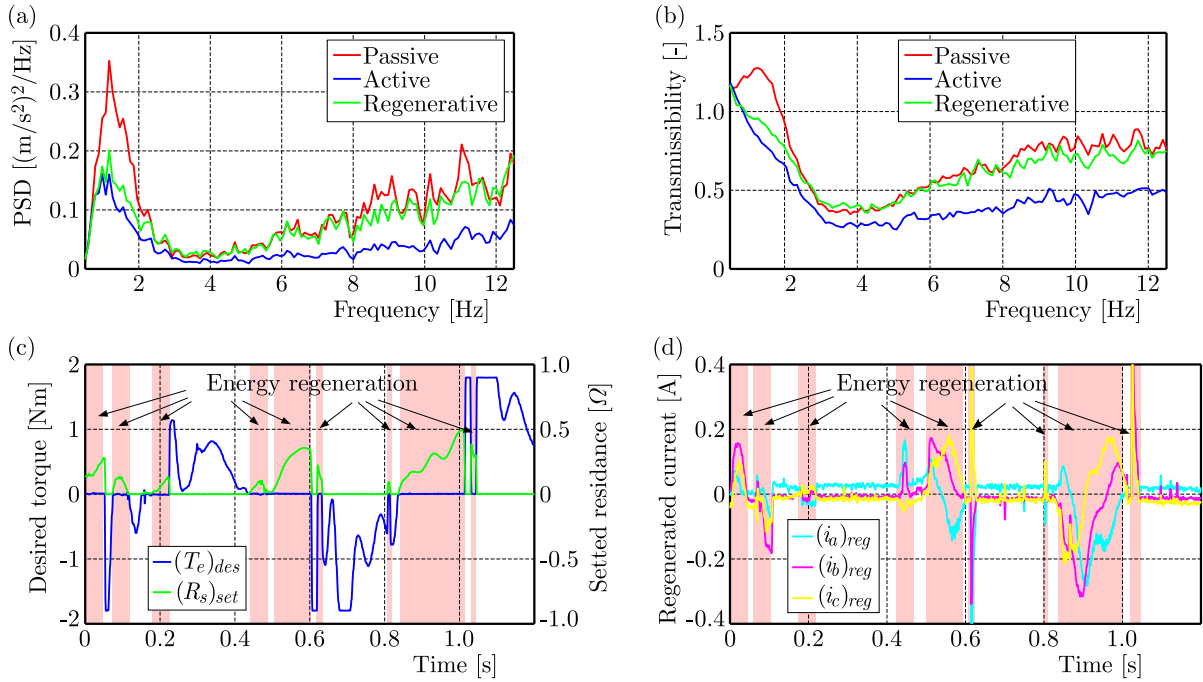

Fig. 6. Measured power spectral densities (a) and transmissibility functions (b) of the passive, active and regenerative suspension system, time histories of the desired motor torque versus the set resistance (c) and the corresponding regenerated phase currents (d)

At the same time on the test-rig, other essential parameters related to the regenerative seat suspension were measured (Figs. 6c and 6d). Figure 6c shows the desired torque generating during the damping period defined by the "motoring" condition in Eq. (2.4). In this figure, the torque values appear by multiplication by r_e the desired force (Fig. 1). The damping periods are marked with white vertical stripes along the selected 1.2 s time sample. On other the hand, pink stripes in Fig. 6c indicate the regenerative period. Particularly, it presents the resistance settled when the motor phases are shortened through the breaking resistors (Fig. 3). The current sensors shown in Fig. 3 measured the current values presented in Fig. 6d in pink strips time periods.

Figures 7a-f show the results of simulation of the passive, active and regenerative suspension system. In Fig. 7a, the power spectral densities of the three systems are compared, showing that the active system has the lowest vibration level (close to experimental results). In the case of regenerative and passive ones, the model returned higher values. The frequency limit 3 Hz is visible like in the case of the experiment. Above this limit, all simulated systems gave very similar results, differently than in the experiment. In Fig. 7b, the transmissibility functions of the three systems are plotted, indicating a similar to power density functions isolation performance of all systems. In this case, however, it should be noted that the regenerative system, in the range up to 3 Hz, reaches values greater than 1, contrary to what the experiment showed. In Fig. 7c, the
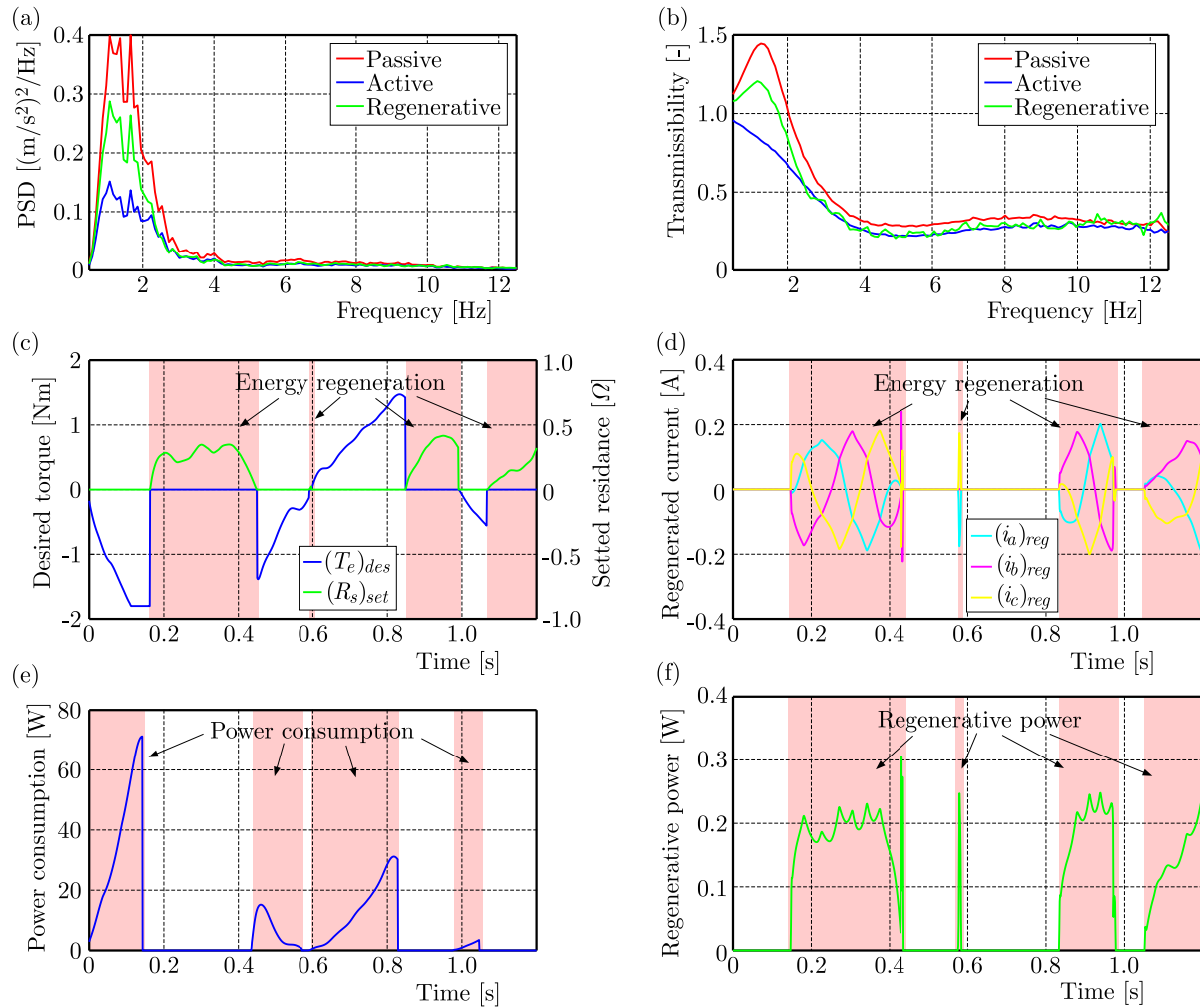
Fig. 7. Simulated power spectral densities (a) and transmissibility functions (b) of the passive, active and regenerative suspension system, time histories of the desired motor torque versus the set resistance (c) and the corresponding regenerated phase currents (d), power consumption (e) and the obtained regenerative power of the electric motor (f)

desired motor torque and the set resistance are shown, demonstrating that the motor torque is zero in the energy regeneration periods contrary to the resistance (pink strips). The opposite is true in the ranges marked by white strips. This confirms the validity of the regenerative model. In Fig. 7d, the phase currents of the electric motor are displayed, revealing that they are in phase with the motor torque. In Fig. 7e, the power consumption of the electric motor is calculated, proving that it is lower than the active system. In Fig. 7f, the regenerative power of the electric motor is estimated, showing that it can recover some energy from the suspension vibration.

5. Conclusions

The experimental study demonstrated that the energy regenerative suspension system can improve the suspension travel and reduce the seat movement limits compared to the passive system, while sacrificing some of the vibration isolation efficiency compared to the active system. The power spectral density and transmissibility function graphs showed the frequency ranges where the regenerative system performed better or similar to the passive system. The test-rig experiment demonstrated the feasibility of the proposed regenerative seat suspension system. The

torque and current measurements confirmed the energy harvesting potential during regenerative periods, as well as the damping performance during motoring periods. The results also validated the mathematical model and the control strategy of the system. In the case of biomechanical modelling, the proposed model is a simplified representation of the human body response to seat vibration, based on a three mass system. The model parameters were obtained by experimental tests and optimisation methods, using the Root Mean Square Error to minimise the discrepancy between simulation and measurement. The model can be used to evaluate the vibration comfort and performance of different seat suspension designs and control strategies. In this work, the operation of the seat suspension together with a human being presence was simulated. The simulation results of the passive, active and regenerative suspension systems were consistent with the experimental ones in terms of vibration reduction and energy recovery. The active system had the best performance in terms of vibration isolation, while the regenerative system had the advantage of lower power consumption and partial energy regeneration. The regenerative model was validated by comparison of the motor torque, resistance, phase currents and power of the electric motor. The simulation results also showed the influence of the frequency limit on the transmissibility and power spectral density functions of the three systems. The results suggest that the regenerative system can be a viable alternative to the active system, especially for applications where energy saving is important and vibration isolation is not critical.

Appendix A. Constant model parameters of a seated human body with horizontal seat suspension and energy recovery braking subsystem

Parameter	Value	Unit
Human body model		
Mass of pelvis m_1	25.18	kg
Mass of torso m_2	46.77	kg
Mass of head m_3	8.04	kg
Damping between pelvis and torso d_{12}	582	Ns/m
Stiffness between pelvis and torso c_{12}	15815	N/m
Damping between torso and head d_{23}	59	Ns/m
Stiffness between torso and head c_{23}	5809	N/m
Damping between torso and backrest d_2	5	Ns/m
Stiffness between torso and backrest c_2	50	N/m
Model of horizontal seat suspension		
Damping of suspension mechanism d_s	1000	Ns/m
Stiffness of suspension mechanism c_s	10000	N/m
Friction coefficient of suspension mechanism μ_s	0.05	–
Lever arm of motor r_e	0.045	m
Model of electrical subsystem		
Number of pole pairs p	3	–
Amplitude of flux induced by permanent magnets λ	0.00733	Vs
Inductance of stator windings L_e	0.0001	H
Resistance of stator windings R_e	0.0675	Ω
Coefficient of maximum braking force k_{max}	1	–

References

1. AKINAGA H., 2020, Recent advances and future prospects in energy harvesting technologies, *Japanese Journal of Applied Physics*, **59**, 110201

2. ALHAJRI I.H., GADALLA M.A., ELAZAB H.A., 2021, A conceptual efficient design of energy recovery systems using a new energy-area key parameter, *Energy Reports*, **7**, 1079-1090

3. ARAUJO M., NICOLETTI R., 2015, Electromagnetic harvester for lateral vibration in rotating machines, *Mechanical Systems and Signal Processing*, **52**, 685-699

4. BEEBY S., TUDOR M.J., WHITE N., 2006, Energy harvesting vibration sources for microsystems applications, *Measurement Science and Technology*, **17**, R175"R195

5. BOUENDEU E., GREINER A., SMITH, P., KORVINK J., 2011, Design synthesis of electromagnetic vibration-driven energy generators using a variational formulation, *Journal of Microelectromechanical Systems*, **20**, 466-475

6. BRAVO R.R.S., DE NEGRI V.J., OLIVEIRA A.A.M., 2018, Design and analysis of a parallel hydraulic – pneumatic regenerative braking system for heavy-duty hybrid vehicles, *Applied Energy*, **225**, 60-77

7. CIPOLLETTA G., DELLE FEMINE A., GALLO D., LUISO M., LANDI C., 2021, Design of a stationary energy recovery system in rail transport, *Energies*, **14**, 9, 2560

8. FARGHALI M., OSMAN A.I., MOHAMED I.M.A., CHEN Z., CHEN L., *et al.*, Strategies to save energy in the context of the energy crisis: a review, *Environmental Chemistry Letters*, **21**, 2003-2039

9. FASTIER-WOOLLER J.W., VU T.-H., NGUYEN H., NGUYEN H.-Q., RYBACHUK M., *et al.*, 2022, Multimodal fibrous static and dynamic tactile sensor, *ACS Applied Materials and Interfaces*, **14**, 27317-27327

10. FATHABADI H., 2019, Recovering waste vibration energy of an automobile using shock absorbers included magnet moving-coil mechanism and adding to overall efficiency using wind turbine, *Energy*, **189**, 116274

11. GABRIEL-BUENAVENTURA A., AZZOPARDI B., 2015, Energy recovery systems for retrofitting in internal combustion engine vehicles: A review of techniques, *Renewable and Sustainable Energy Reviews*, **41**, 955-964

12. GODFREY J.A., SANKARANARAYANAN V., 2018, A new electric braking system with energy regeneration for a BLDC motor driven electric vehicle, *Engineering Science and Technology, an International Journal*, **21**, 4, 704-713

13. HALIM M.A., CHO H., SALAUDDIN M., PARK J.Y., 2016, A miniaturized electromagnetic vibration energy harvester using flux-guided magnet stacks for human-body-induced motion, *Sensors and Actuators A: Physical*, **249**, 23-29

14. HU Y.T., XUE H., HU H.P., 2013, Piezoelectric power/energy harvesters, [In:] *Analysis of Piezoelectric Structures and Devices*, Chapter 3, D. Fang, J. Wang, W. Chen (Edit.), De Gruyter: Berlin, Germany, 72-75

15. JERECZEK B., MACIEJEWSKI I., KRZYŻYŃSKI T., KRÓLIKOWSKI T., 2022, Modeling and simulation of the horizontal seat suspension system under random vibration, *Procedia Computer Science*, **207**, 858-866

16. JIANG J., LIU S., FENG L., ZHAO D., 2021, A review of piezoelectric vibration energy harvesting with magnetic coupling based on different structural characteristics, *Micromachines*, **12**, 4, 436

17. KRAUSE P.C., WASYNCZUK O., SUDHOFF S.D., 2002, *Analysis of Electric Machinery and Drive Systems*, Wiley-IEEE Press

18. KIM T., 2011, Regenerative braking control of a light fuel cell hybrid electric vehicle, *Electric Power Components and Systems*, **39**, 5, 446-460

19. Li L., Ping X., Shi J., Wang X., Wu X., 2021, Energy recovery strategy for regenerative braking system of intelligent four-wheel independent drive electric vehicles, *IET Intelligent Transport Systems*, **15**, 1, 119-131

20. Liu C., Zhang K., 2021, Research on regenerative braking energy recovery strategy of electric vehicle, *Journal of Physics: Conference Series*, **2030**, 1, 012003

21. Maciejewski I., Blazejewski A., Pecolt S., Krzyzynski T., 2022a, A sliding mode control strategy for active horizontal seat suspension under realistic input vibration, *Journal of Vibration and Control*, **29**, 11-12, 25392551

22. Maciejewski I., Błażejewski A., Pecolt S., Królikowski T., 2022b, Multi-body model simulating biodynamic response of the seated human under whole-body vibration, *Procedia Computer Science*, **207**, 227-234

23. Maciejewski I., Błażejewski A., Pecolt S., Krzyżyński T., Zaporski P., 2023, Three-dimensional modelling and parameter identification of the seated human body exposed to random vibration, *Journal of Theoretical and Applied Mechanics*, **61**, 4, 833-845

24. Maciejewski I., Glowinski S., Krzyzynski T., 2014, Active control of a seat suspension with the system adaptation to varying load mass, *Mechatronics*, **24**, 8, 1242-1253

25. Maciejewski I., Zlobinski M., Krzyzynski T., Glowinski S., 2020, Vibration control of an active horizontal seat suspension with a permanent magnet synchronous motor, *Journal of Sound and Vibration*, **488**, 115655

26. Matak M., Solek P., 2013, Harvesting the vibration energy, *American Journal of Mechanical Engineering*, **7**, 438-442

27. Mescia L., Losito O., Prudenzano F., 2015, *Innovative Materials and Systems for Energy Harvesting Applications*, IGI Global: Hershey, PA, USA, 254-259, 271-272

28. Muscat A., Bhattacharya S., Zhu Y., 2022, Electromagnetic vibrational energy harvesters: A review, *Sensors*, **22**, 15, 5555

29. Naseri F., Farjah E., Ghanbari T., 2017, An efficient regenerative braking system based on battery/supercapacitor for electric, hybrid, and plug-in hybrid electric vehicles with BLDC motor, *IEEE Transactions on Vehicular Technology*, **66**, 5, 3724-3738

30. Onar O.C., Khaligh A., 2012, A novel integrated magnetic structure based DC/DC converter for hybrid battery/ultracapacitor energy storage systems, *IEEE Transactions on Smart Grid*, **3**, 1, 296-307

31. Priya S., Song H., Zhou Y., Varghese R., Chopra A., *et al.*, 2017, A review on piezoelectric energy harvesting, materials, methods, and circuits, *Energy Harvesting and Systems*, **4**, 3-39

32. Salman W., Qi L., Zhu X., Pan H., Zhang X., *et al.*, 2018, A high-efficiency energy regenerative shock absorber using helical gears for powering low-wattage electrical device of electric vehicles, *Energy*, **159**, 361-372

33. Song Z., Li J., Han X., Xu L., Lu L., *et al.*, 2014, Multi-objective optimization of a semi-active battery/supercapacitor energy storage system for electric vehicles, *Applied Energy*, **135**, 212-224

34. Sudevalayam S., Kulkarni P., 2011, Energy harvesting sensor nodes: Survey and implications, *IEEE Communications Surveys and Tutorials*, **13**, 443-461

35. Taut A., Pop O., Ceuca E., 2013, System for energy recovering with BLDC motor at deceleration momentum, *Proceedings of the 36th International Spring Seminar on Electronics Technology*, 299-304

36. Toshiyoshi H., Ju S., Honma H., Ji C.-H., Fujita H., 2019, MEMS vibrational energy harvesters, *Science and Technology of Advanced Materials*, **20**, 124-143

37. Ueno T., 2019, Magnetostrictive vibrational power generator for battery-free IoT application, *AIP Advances*, **9**, 035018

38. Wang X., 2020, Research on track vibration energy recovery system for vehicle operation based on network system, *Journal of Physics: Conference Series*, **1574**, 1, 012055

39. Yang Y.P., Liu J.J., Wang T.J., Kuo K.C., Hsu P.E., 2007, An electric gearshift with ultracapacitors for the power train of an electric vehicle with a directly driven wheel motor, *IEEE Transactions on Vehicular Technology*, **56**, 5, 2421-2431

40. Zhang R., Wang C., Zou P., Lin R., Ma L., *et al.*, 2022, Compositionally complex doping for zero-strain zero-cobalt layered cathodes, *Nature*, **610**, 67-73

41. Zhu Y., Moheimani S.O.R., Yuce M.R., 2010a, A 2-DOF MEMS ultrasonic energy harvester, *IEEE Sensors Journal*, **11**, 155-161

42. Zhu Y., Moheimani S., Yuce M., 2010b, Ultrasonic energy transmission and conversion using a 2-D MEMS resonator, *IEEE Electron Device Letters*, **31**, 374-376